Chemical Science

ROYAL SOCIETY OF CHEMISTRY

EDGE ARTICLE

View Article Online
View Journal | View Issue

Check for updates

Cite this: *Chem. Sci.*, 2022, **13**, 11600

All publication charges for this article have been paid for by the Royal Society of Chemistry

Received 2nd June 2022
Accepted 12th September 2022

DOI: 10.1039/d2sc03089f

rsc.li/chemical-science

Open Access Article. Published on 13 September 2022. Downloaded on 2/12/2026 9:22:40 AM. This article is licensed under a Creative Commons Attribution-NonCommercial 3.0 Unported Licence.

Synergistic effects of CH_3CO_2H and Ca^{2+} on C–H bond activation by MnO_4^-†

Huatian Shi,‡ Lin Cheng,‡ Yi Pan, Chi-Keung Mak,* Kai-Chung Lau * and Tai-Chu Lau *

The activation of metal-oxo species with Lewis acids is of current interest. In this work, the effects of a weak Brønsted acid such as CH_3CO_2H and a weak Lewis acid such as Ca^{2+} on C–H bond activation by $KMnO_4$ have been investigated. Although MnO_4^- is rather non-basic (pK_a of $MnO_3(OH) = -2.25$), it can be activated by AcOH or Ca^{2+} to oxidize cyclohexane at room temperature to give cyclohexanone as the major product. A synergistic effect occurs when both AcOH and Ca^{2+} are present; the relative rates for the oxidation of cyclohexane by MnO_4^-/AcOH, MnO_4^-/Ca^{2+} and MnO_4^-/AcOH/Ca^{2+} are 1 : 73 : 198. DFT calculations show that in the active intermediate of MnO_4^-/AcOH/Ca^{2+}, MnO_4^- is H-bonded to 3 AcOH molecules, while Ca^{2+} is bonded to 3 AcOH molecules as well as to an oxo ligand of MnO_4^-. Our results also suggest that these synergistic activating effects of a weak Brønsted acid and a weak Lewis acid should be applicable to a variety of metal-oxo species.

Introduction

The chemistry of metal-oxo species has been of great interest to chemists because of the key roles they play in various chemical and biological systems.[1–4] In recent years, the use of Lewis acids to enhance the reactivity of metal-oxo species has attracted much attention,[5,6] especially after the discovery of a Ca^{2+} in the active site of the oxygen-evolving center (OEC) of photosystem II, which contains a manganese calcium oxo cluster (Mn_4CaO_5).[7,8]

Various metal-oxo species are readily activated by strong Lewis acids such as BF_3, $Sc(OTf)_3$ and other M^{3+} ions toward the oxidation of organic substrates.[9–19] There are also a number of studies on the interaction of relatively weak Lewis acids such as Ca^{2+} and other group II ions with metal-oxo species, and as expected their activating effects are much smaller than those of $Sc(OTf)_3$ or other M^{3+} ions.[12,15,20–24]

We recently reported the use of a weak Brønsted acid such as acetic acid in combination with a weak Lewis acid such as a group II ion to activate RuO_4^-.[25] We found a remarkable cooperative activating effect of these two acids on RuO_4^- toward the oxidation of alkanes. The oxo ligands in RuO_4^- are basic and can be protonated by AcOH to generate $[RuO_3(OH)]OAc^-$, which readily abstracts H atoms from alkanes. In the presence of Ca^{2+}, a more active intermediate is formed with $[RuO_3(OH)]OAc^-$, in which Ca(II) binds to both OAc^- (which is H-bonded to OH) and an oxo ligand. In this work, we have carried out experimental and theoretical investigations on the use of AcOH and Ca^{2+} to activate MnO_4^- toward cyclohexane oxidation. MnO_4^- was chosen because of the relevance of Mn in the OEC of photosystem II. Remarkably, a similar synergistic activating effect of AcOH and Ca^{2+} is also observed for this oxoanion, although MnO_4^- is much less basic than RuO_4^- and is not protonated by AcOH. Our results suggest that the synergistic effects of a weak Brønsted and a weak Lewis acid should be applicable to a variety of metal-oxo species.

Department of Chemistry, City University of Hong Kong, Tat Chee Avenue, Kowloon Tong, Hong Kong, China. E-mail: bhtclau@cityu.edu.hk; kaichung@cityu.edu.hk; chikmak6@cityu.edu.hk

† Electronic supplementary information (ESI) available. See https://doi.org/10.1039/d2sc03089f

‡ These authors have equal contribution.

Results and discussion

Effects of AcOH on cyclohexane oxidation by $KMnO_4$

$KMnO_4$ does not react with cyclohexane at room temperature. However, upon addition of AcOH (3–9 M) to $KMnO_4$ (0.011 M) in CH_3CN in the presence of cyclohexane (1.0 M) at 23 °C, the purple color of the solution gradually changed to brown. Analysis of the solution by GC-MS and GC-FID revealed the formation of cyclohexanone (38.8%), together with a small amount of cyclohexanol (2.2%). The yields were calculated based on $KMnO_4$ acting as a 3-electron oxidant (product is a Mn(IV) species, see below).

Kinetics studies were carried out at constant [$KMnO_4$] (0.011 M) and [cyclohexane] (1.0 M) by monitoring the growth of cyclohexanone using a GC-FID (gas chromatograph-flame ionization detector). The increase in [cyclohexanone] follows pseudo-first-order kinetics (Fig. 1a), and the pseudo-first-order rate constant k_{obs} at [AcOH] = 3.0 M was found to be 4.3×10^{-6} s^{-1}. k_{obs} increases with increasing [AcOH] (3–9 M), and the plot of k_{obs} *versus* [AcOH]^2 is linear (Fig. 1b), suggesting that

© 2022 The Author(s). Published by the Royal Society of Chemistry

Open Access Article. Published on 13 September 2022. Downloaded on 2/12/2026 9:22:40 AM. This article is licensed under a Creative Commons Attribution-NonCommercial 3.0 Unported Licence.

under these conditions the active oxidizing species involves MnO_4^- binding to two molecules of AcOH. The reaction can be represented by eqn (1) and (2).

$$MnO_4^- + 2AcOH \overset{K_1}{\rightleftharpoons} MnO_4^- \cdot 2AcOH \quad (1)$$

$$MnO_4^- \cdot 2AcOH + c\text{-}C_6H_{12} \xrightarrow{k_a} Product \quad (2)$$

Under the condition that $K_1 \ll 1$, the rate-law is given by eqn (3).

$$d[C_6H_{10}O]/dt = k_{obs}[MnO_4^-] = K_1k_a[AcOH]^2[c\text{-}C_6H_{12}][MnO_4^-] \quad (3)$$

From the slope of Fig. 1b, $K_1k_a = (4.73 \pm 0.19) \times 10^{-7}$ M^{-2} s^{-1} at 23.0 °C.

The kinetic isotope effect for cyclohexane oxidation determined by competitive oxidation of an equimolar mixture of c-C_6H_{12} and c-C_6D_{12} was found to be 7.5 ± 0.1, indicating C–H bond cleavage in the rate-limiting step.

Effects of Ca^{2+}

The oxidation of cyclohexane by $KMnO_4$ is also activated by Ca^{2+}. Upon adding $Ca(OTf)_2$ (5.5×10^{-3} to 4.4×10^{-2} M) to $KMnO_4$ (0.011 M) in CH_3CN containing cyclohexane (1.0 M), the purple color of the solution was gradually discharged together with the formation of a brown precipitate (Fig. 2). The UV/vis spectral changes indicate that there is no shift in the wavelengths of the peaks of MnO_4^-, just a gradual decrease in their absorbances (Fig. S1†). The same result was also observed in our earlier work on the effect of BF_3 on $KMnO_4$.[18] The solution IR of $KMnO_4$ and $KMnO_4$ + $Ca(OTf)_2$ in CH_3CN was also performed (Fig. S2†). $KMnO_4$ shows a M=O stretch at 904 cm^{-1}, but this peak was not shifted upon addition of $Ca(OTf)_2$; presumably the binding of Ca^{2+} to MnO_4^- is relatively weak.

Analysis of the product solution by GC-FID and GC-MS revealed the formation of cyclohexanone (10.5%) and cyclohexanol (0.8%) in relatively low yields. The yields of products reached a maximum with just 1 equiv. of Ca^{2+}.

Kinetics studies were also carried out at various $[Ca(OTf)_2]$ but at constant $[KMnO_4]$ (0.011 M) and [cyclohexane] (1.0 M). The increase in [cyclohexanone] follows pseudo-first-order kinetics (Fig. 3a), but saturation kinetics were observed on increasing $[Ca(OTf)_2]$ (Fig. 3b), and the plot of $1/k_{obs}$ *versus* $1/[Ca(OTf)_2]$ is linear. Kinetic studies were also conducted at various [cyclohexane] (Fig. 4a), while keeping both $Ca(OTf)_2$ and $KMnO_4$ at 0.011 M. The plot of k_{obs} *versus* [cyclohexane] is linear with an intercept of $(2.87 \pm 3.3) \times 10^{-4}$ s^{-1} (Fig. 4b), which should be due to the decomposition of $KMnO_4$ in the absence of cyclohexane. An independent experiment showed that in the presence of 1 equiv. of $Ca(OTf)_2$, the absorbance of $KMnO_4$ (2.82×10^{-4} M) in CH_3CN at around 527 nm gradually decreased with time with a rate constant of $(9.5 \pm 1.1) \times 10^{-4}$ s^{-1} at 23 °C. Such a decomposition also accounts for the low yield of products. The kinetic results are consistent with a pre-equilibrium binding of Ca(II) to MnO_4^- to form an intermediate, which then oxidizes cyclohexane, as represented by eqn (4) and (5), and the rate law is shown in eqn (6).

$$Ca(OTf)_2 + MnO_4^- \overset{K_2}{\rightleftharpoons} [Ca(OTf)_2 \cdot MnO_4^-] \quad (4)$$

$$[Ca(OTf)_2 \cdot MnO_4^-] + c\text{-}C_6H_{12} \xrightarrow{k_b} Product \quad (5)$$

$$\frac{d[C_6H_{10}O]}{dt} = k_{obs}[MnO_4^-] = \frac{k_bK_2[Ca(OTf)_2]}{(1 + K_2[Ca(OTf)_2])}[c\text{-}C_6H_{12}][MnO_4^-] \quad (6)$$

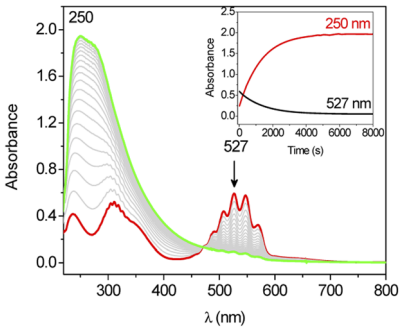

Fig. 2 UV-vis spectral changes for the reaction of $KMnO_4$ (2.35×10^{-3} M) with cyclohexane (1.0 M) in the presence of $Ca(OTf)_2$ (2.35×10^{-3} M) in CH_3CN at 25 °C (1 mm UV cell was used in the measurement). The inset shows the change of absorbance at 250 nm and 527 nm *versus* time.

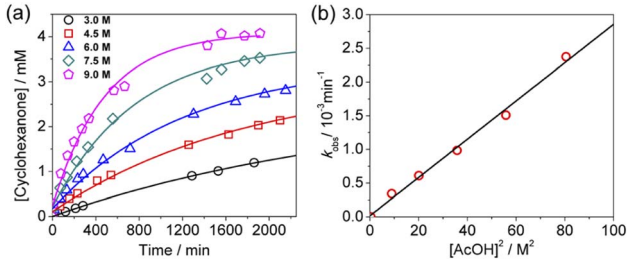

Fig. 1 (a) Time course for the production of cyclohexanone at various [AcOH]. Conditions: $KMnO_4$, 0.011 M; cyclohexane, 1.0 M; at 23 °C in CH_3CN. (b) Linear plot of k_{obs} *vs.* $[AcOH]^2$. Slope = $(2.84 \pm 0.11) \times 10^{-5}$, intercept = $(2 \pm 5) \times 10^{-5}$, and $r^2 = 0.992$.

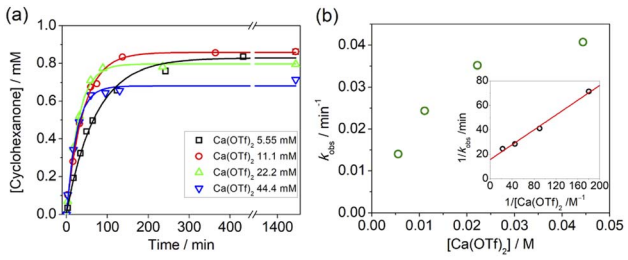

Fig. 3 (a) Time course for the production of cyclohexanone at various $[Ca(OTf)_2]$. Conditions: $KMnO_4$, 0.011 M; cyclohexane, 1.0 M; at 23 °C in CH_3CN. (b) Plot of k_{obs} *versus* $[Ca(OTf)_2]$. Inset: linear plot of $1/k_{obs}$ *vs.* $1/[Ca(OTf)_2]$; slope = 0.303 ± 0.018, intercept = 15.8 ± 1.9, and r^2 = 0.99.

Open Access Article. Published on 13 September 2022. Downloaded on 2/12/2026 9:22:40 AM. This article is licensed under a Creative Commons Attribution-NonCommercial 3.0 Unported Licence.

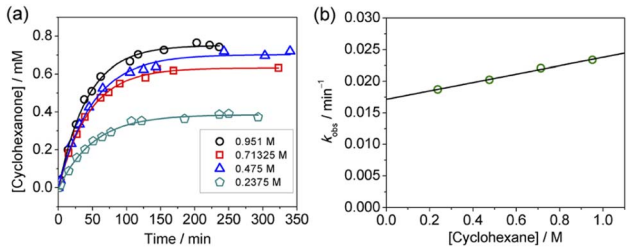

Fig. 4 (a) Time course for the production of cyclohexanone at various [cyclohexane]. Conditions: $KMnO_4$ (0.011 M), $Ca(OTf)_2$ (0.011 M) and cyclohexane (0.238–0.951 M) in CH_3CN at 23 °C. (b) Plot of k_{obs} *vs.* [cyclohexane]. Slope = (6.64 ± 0.29) × 10^{-3}, intercept = (1.72 ± 0.02) × 10^{-2}, and r^2 = 0.994.

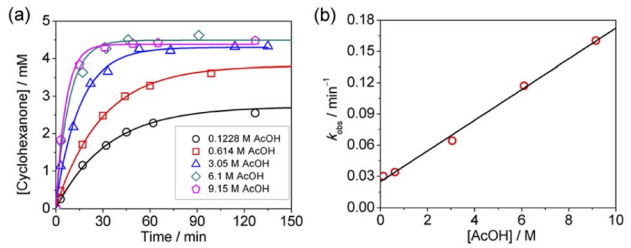

Fig. 5 (a) Time course for cyclohexanone production by $KMnO_4$ (0.011 M) in the presence of cyclohexane (1.0 M), 1 equiv. of $Ca(OTf)_2$ (0.011 M) and various [AcOH] in CH_3CN at 23.0 °C. (b) Plot of k_{obs} *vs.* [AcOH]. Slope = (1.56 ± 0.06) × 10^{-2}, *y*-intercept = 0.025 ± 0.003, and r^2 = 0.995.

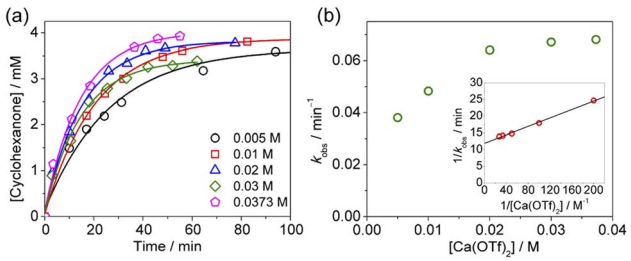

Fig. 6 (a) Time course for cyclohexane production in CH_3CN at various [$Ca(OTf)_2$]. Conditions: cyclohexane, 1.0 M; $KMnO_4$, 0.011 M; AcOH, 2.79 M. T = 23 °C. (b) Plot of k_{obs} *versus* [$Ca(OTf)_2$]. Inset: plot of 1/k_{obs} *versus* 1/[$Ca(OTf)_2$]; slope = (6.3 ± 0.2) × 10^{-2}, *y*-intercept = 11.9 ± 0.2, and r^2 = 0.995.

K_2 = *y*-intercept/slope of Fig. 3b = (52.1 ± 3.5) M^{-1} and k_b = 1/*y*-intercept = (1.1 ± 0.1) × 10^{-1} M^{-3} s^{-1} at 23 °C.

Synergistic effects of AcOH and Ca^{2+}

The oxidation of cyclohexane in the presence of both AcOH and Ca^{2+} was investigated. As described above, the rate of oxidation of cyclohexane by $KMnO_4$/AcOH is second-order in [AcOH]. However, in the presence of just 1 equiv. of $Ca(OTf)_2$, the rate becomes first-order in [AcOH] (Fig. 5).

On the other hand, at constant [AcOH] (2.79 M) and [cyclohexane] (1.0 M), saturation kinetics were observed on increasing [$Ca(OTf)_2$], and the plot of 1/k_{obs} *versus* 1/[$Ca(OTf)_2$] is linear (Fig. 6).

These results are consistent with the reaction scheme shown in eqn (7)–(9).

$$MnO_4^- + AcOH \overset{K_3}{\rightleftharpoons} [MnO_4^- \cdot AcOH] \quad (7)$$

$$[MnO_4^- \cdot AcOH] + Ca(OTf)_2 \overset{K_4}{\rightleftharpoons} [MnO_4^- \cdot AcOH \cdot Ca(OTf)_2] \quad (8)$$

$$[MnO_4^- \cdot AcOH \cdot Ca(OTf)_2] + c\text{-}C_6H_{12} \xrightarrow{k_c} Product \quad (9)$$

For $K_3 \ll 1$, the rate law is

$$\frac{d[C_6H_{10}O]}{dt} = \frac{k_c K_3 K_4 [Ca(OTf)_2]}{(1 + K_4[Ca(OTf)_2])}[AcOH][MnO_4^-][c\text{-}C_6H_{12}] = k_{obs}[MnO_4^-] \quad (10)$$

K_4 = *y*-intercept/slope of Fig. 6b insett = 188.9 ± 5.6 M^{-1}. From the slope of Fig. 5b and using [$Ca(OTf)_2$] = 0.011 M, K_3k_c was calculated to be (3.85 ± 0.15) × 10^{-4} M^{-1} s^{-1} (23 °C).

The kinetic isotope effect for cyclohexane oxidation by the $KMnO_4$/AcOH/$Ca(OTf)_2$ system was determined to be 5.7 ± 0.1 by competitive oxidation of an equimolar mixture of c-C_6H_{12} and c-C_6D_{12}, indicating that C–H bond cleavage is the rate limiting step.

A comparison of the activating effects of AcOH, $Ca(OTf)_2$ and AcOH + $Ca(OTf)_2$ on cyclohexane oxidation by $KMnO_4$ is shown in Table 1. The rate constant (k_{obs}) for the oxidation of cyclohexane (1.0 M) by $KMnO_4$ (0.011 M) in the presence of AcOH (3.0 M) at 23 °C was found to be 5.73 × 10^{-6} s^{-1}. When AcOH was replaced by 1 equiv. of $Ca(OTf)_2$ (0.011 M), the rate constant

Table 1 Effects of AcOH, $Ca(OTf)_2$ and AcOH + $Ca(OTf)_2$ on the oxidation of cyclohexane by $KMnO_4$ in CH_3CN at 23 °C[a,b]

	3.0 M AcOH (275 equiv.)	1 equiv. $Ca(OTf)_2$ (0.011 M)	1 equiv. $Ca(OTf)_2$ + 3.0 M of AcOH
k_{obs} (relative rate)	5.73 × 10^{-6} s^{-1} (1)	4.21 × 10^{-4} s^{-1} (73)	1.14 × 10^{-3} s^{-1} (198)
Oxidation state of Mn product[c]	4.1 ± 0.2	4.1 ± 0.2	4.0 ± 0.2
% Yield of cyclohexanone[d]	38.8	10.5	57.3
Cyclohexanone/cyclohexanol	18 ± 1	14 ± 1	7 ± 1

[a] Reaction conditions: $KMnO_4$, 0.011 M, cyclohexane, 1.0 M, T = 23 °C. [b] $KMnO_4$ alone does not oxidize cyclohexane for >48 h at 23 °C. [c] The final oxidation state of the Mn product after oxidation was determined by iodometric titration. [d] % Yield was calculated based on $KMnO_4$ acting as a 3-electron oxidant. Cyclohexanol is the minor product in all cases.

© 2022 The Author(s). Published by the Royal Society of Chemistry

Open Access Article. Published on 13 September 2022. Downloaded on 2/12/2026 9:22:40 AM. This article is licensed under a Creative Commons Attribution-NonCommercial 3.0 Unported Licence.

(4.21×10^{-4} s^{-1}) is 73 times faster, but the yield is much lower (10.5%). On the other hand, in the presence of both $Ca(OTf)_2$ and AcOH, the rate (1.14×10^{-3} s^{-1}) increases by 198 fold relative to AcOH alone, and the product yield is also substantially increased to 57%, indicating synergistic effects of AcOH and Ca^{2+} in the activation of MnO_4^- toward C–H bond activation.

The rate constant for the oxidation of 1.0 M toluene by ($^nBu_4N$)MnO_4 was reported to be 4.2×10^{-7} s^{-1} at 25.0 °C.[26] As a comparison, we also investigated the oxidation of 1.0 M toluene by $KMnO_4$ in the presence of 1 equiv. $Ca(OTf)_2$ and 3.0 M AcOH, and the rate constant was found to be 5.2×10^{-3} s^{-1} at 23 °C (Fig. S3†). Based on these data, the oxidation of toluene by $KMnO_4/Ca^{2+}$/AcOH is over 4 orders of magnitude faster than that of MnO_4^- alone.

Effects of other metal ions

The effects of other metal salts, including $Ba(OTf)_2$, $Mg(OTf)_2$, and $Sc(OTf)_3$ on cyclohexane oxidation by $KMnO_4$ in the presence of AcOH have also been investigated. As expected, both the rate and yield increase with increasing Lewis acidity of the metal ion (Fig. 7a and S4–S6†). The ratio of the rate constants obtained by GC for the 4 metal ions is found to be $k(Ba^{2+}) : k(Ca^{2+}) : k(Mg^{2+}) : k(Sc^{3+}) = 1 : 4.8 : 10.4 : 228$; and the yields of cyclohexanone are 51%(Ba^{2+}), 56%(Ca^{2+}), 61%(Mg^{2+}), and 75%(Sc^{3+}). There is a fairly linear correlation of log(rate constant) with the pK_a of the metal ion in water, Sc^{3+}(pK_a = 4.3), Mg^{2+}(pK_a = 11.2), Ca^{2+}(pK_a = 12.7), and Ba^{2+}(pK_a = 13.4),[27] which is a measure of their Lewis acidity (Fig. 7b). Similar correlations of Lewis acid effects with their acidities have also been reported.[15,23]

Nature of the manganese product

Addition of $Ca(OTf)_2$ to $KMnO_4$ in CH_3CN gradually produced a brown solid and a colorless solution, irrespective of whether cyclohexane was present. When AcOH (3 M) was added to the resulting solution after cyclohexane oxidation, the brown solid dissolved but with only a small increase of 1–2% cyclohexanone. The oxidation state of Mn in the brown solution was determined to be 4.1 ± 0.2 by iodometric titration, which involves the addition of NBu_4I to reduce the Mn^n product to Mn^{II} and then determining the amount of I_3^- formed by UV-vis spectrophotometry.[28]

Based on CHN elemental analysis, as well as K, Mn and Ca analysis by ICP-AES, it was found that the brown solids obtained from $MnO_4^-/Ca(OTf)_2$ (**1**) and $MnO_4^-/Ca(OTf)_2$/c-C_6H_{12} (**2**) have similar compositions and are probably a Mn^{IV}–μ(O)–μ(Ca) polymer with an empirical formula close to "$Ca_3Mn_7O_{14}(H_2O)_{10}(OTf)_6(CH_3CN)_2$" (see the ESI†). The reason for the conversion of Mn^{VII} to Mn^{IV} in the absence of c-C_6H_{12} is not clear, presumably due to oxidation of the solvent.

We have carried out X-ray photoelectron spectroscopy (XPS) of **1** and **2** (Fig. S7 and S8†). In the Mn3s XPS spectra (Fig. S8†), the peak splitting of ΔE = 4.8 eV indicates that the oxidation state of Mn is +4.[29]

We have also determined the magnetic susceptibility of the solid samples of **1** and **2** using a magnetic balance. The μ_{eff} for each Mn was found to be 3.96 and 4.05 μ_B for **1** and **2**, respectively, consistent with that of high spin Mn(IV) with S = 3/2.

No brown precipitate was observed when cyclohexane oxidation was carried out in the presence of AcOH, irrespective of whether $Ca(OTf)_2$ was added. The Mn oxidation state of the brown solution determined by iodometric titration is again 4.0 ± 0.2. Presumably the brown solution contains colloidal MnO_2, as observed in alkane oxidation by BF_3/MnO_4^-.[18]

Theoretical calculations

DFT calculations on the mechanisms of the oxidation of cyclohexane by MnO_4^-, MnO_4^-/AcOH, $MnO_4^-/Ca(OTf)^+$ and MnO_4^-/AcOH/$Ca(OTf)^+$ were performed. Solvent (CH_3CN) effects have been included in the calculations.

The potential energy surfaces (PESs) for all calculated reactions are summarized in Fig. S9.† In the c-C_6H_{12} oxidation by MnO_4^- in CH_3CN (Fig. 8), c-C_6H_{12} and MnO_4^- first bind weakly together to form an intermediate $[MnO_4\cdots C_6H_{12}]^-$, INT1($MnO_4^-$). Hydrogen atom transfer (HAT) then occurs from

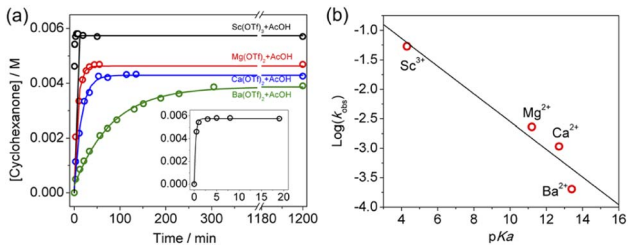

Fig. 7 (a)Time course for the production of cyclohexanone by $KMnO_4$ (0.01 M)/AcOH (2.78 M)/c-C_6H_{12} (1.0 M) in the presence of 0.01 M of various metal salts. Pseudo-first-order fits give k_{obs}: $Sc(OTf)_3$ = 5.4 × 10^{-2} s^{-1}, $Mg(OTf)_2$ = 2.3 × 10^{-3} s^{-1}, $Ca(OTf)_2$ = 1.1 × 10^{-3} s^{-1}, and $Ba(OTf)_2$ = 2 × 10^{-4} s^{-1}. The inset shows the time course for $Sc(OTf)_3$. (b) Plot of log(k_{obs}) *vs.* pK_a of metal ions. Sc^{3+}(pK_a = 4.3), Mg^{2+}(pK_a = 11.2), Ca^{2+}(pK_a = 12.7), and Ba^{2+}(pK_a = 13.4). Slope = −0.24 ± 0.04, intercept = −0.2 ± 0.5, and r^2 = 0.90.

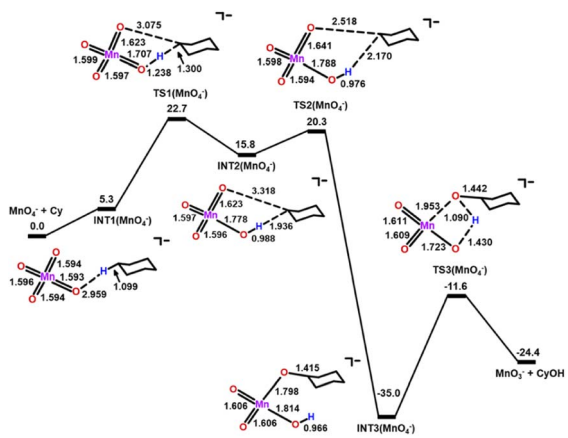

Fig. 8 PES and structures for cyclohexane oxidation by $[MnO_4]^-$ at the B3LYP-D3(BJ)/def2-SVPD level. The relative 298 K Gibbs free energies in acetonitrile are given in kcal mol^{-1}.

Open Access Article. Published on 13 September 2022. Downloaded on 2/12/2026 9:22:40 AM. This article is licensed under a Creative Commons Attribution-NonCommercial 3.0 Unported Licence.

c-C_6H_{12} to Mn=O *via* a transition state, TS1(MnO_4^-), to give a second intermediate, INT2(MnO_4^-). The HAT step is rate-determining with a barrier height ($\Delta G^{\ddagger}_{298}$) of 22.7 kcal mol^{-1}. Such a high barrier suggests that MnO_4^- will hardly oxidize c-C_6H_{12} at room temperature. The carbon atom in the cyclohexyl radical of INT2(MnO_4^-) bears a −1.01 electron spin, consistent with the spin distribution for a HAT. In the next step, the cyclohexyl radical binds to another Mn=O to generate an alkoxo intermediate $[MnO_2(OH)(OC_6H_{11})]^-$ *via* TS2(MnO_4^-). Subsequently, proton transfer from Mn–OH to the alkoxide in INT3(MnO_4^-) occurs *via* TS3(MnO_4^-) to generate the cyclohexanol product. The reaction mechanism is similar to that of c-C_6H_{12} oxidation by RuO_4^- found in our previous study.[25]

In the presence of an acetic acid molecule (Fig. S10†), AcOH and MnO_4^- first form INT1(AcOH), $[MnO_4(AcOH)\cdots C_6H_{12}]^-$, through a hydrogen bond. The Mn=O that is H-bonded to AcOH is elongated to 1.611 Å, while the other three Mn=O bonds become more electrophilic and shorter with distances of 1.587–1.590 Å, compared with the bond length of 1.594 Å in MnO_4^-. In TS1(AcOH), HAT occurs from c-C_6H_{12} to another free but shorter Mn=O bond (bond length = 1.588 Å). The $\Delta G^{\ddagger}_{298}$ of TS1(AcOH) is 20.4 kcal mol^{-1}, which is 2.3 kcal mol^{-1} lower than that of TS1(MnO_4^-). The subsequent steps are similar to those in c-C_6H_{12} oxidation by MnO_4^-.

In the presence of three AcOH molecules, the AcOH molecules form hydrogen bonds with three Mn=O to give an intermediate, INT1(3AcOH) (Fig. 9). The bond lengths of the H-bonded Mn=O are slightly elongated from 1.591 to 1.601 Å. HAT then occurs from c-C_6H_{12} to the free and more electrophilic Mn=O bond (bond length = 1.580 Å), with a $\Delta G^{\ddagger}_{298}$ = 16.8 kcal mol^{-1}. Compared with c-C_6H_{12} oxidation by MnO_4^-, the $\Delta G^{\ddagger}_{298}$ of HAT is further reduced by 5.9 kcal mol^{-1}.

In the presence of $[Ca(OTf)]_2$ (Fig. 10), Ca(II) binds to two of the Mn=O bonds to form INT1(CaOTf), $[MnO_4(CaOTf)\cdots C_6H_{12}]$. The two Mn=O bonds that bind to Ca(II) in INT1(CaOTf) are longer (1.611 and 1.615 Å) than the unbound Mn=O bonds (1.576 Å) in INT1(MnO_4^-), as a result of the electron withdrawing effect of Ca(II). Subsequent HAT from c-C_6H_{12} to an unbound

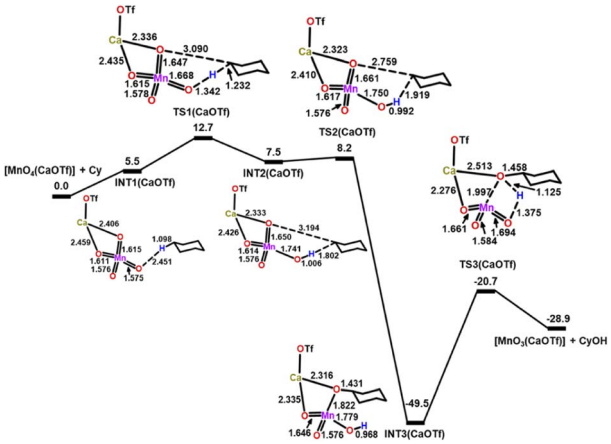

Fig. 10 PES and structures for cyclohexane oxidation by [MnO_4(-CaOTf)] at the B3LYP-D3(BJ)/def2-SVPD level. The relative 298 K Gibbs free energies in acetonitrile are given in kcal mol^{-1}.

Mn=O occurs with a $\Delta G^{\ddagger}_{298}$ of 12.7 kcal mol^{-1} *via* TS1(CaOTf), which is lower than that of MnO_4^- and MnO_4^-/3AcOH by 10.0 and 4.1 kcal mol^{-1}, respectively; consistent with the experimental observation that the accelerating effect of Ca(II) is much higher than that of AcOH.

The activation barrier is further lowered when both $[Ca(OTf)]^+$ and AcOH are present. In the presence of one molecule of $[Ca(OTf)]^+$ and three molecules of AcOH, each AcOH is H-bonded to one Mn=O, while the $[Ca(OTf)]^+$ is bonded to each AcOH and one Mn=O to form a relatively stable intermediate, INT1(CaOTf/3AcOH), as shown in Fig. 11. HAT then occurs from c-C_6H_{12} to the free and shortest Mn=O bond with the lowest $\Delta G^{\ddagger}_{298}$ of 9.7 kcal mol^{-1} ($\Delta G^{\ddagger}_{298}$ = 11.5 kcal mol^{-1} for one $Ca(OTf)^+$ and one AcOH, Fig. S11†), in agreement with the observed synergistic activating effects of AcOH and Ca(II). It should be noted that in this case HAT results in the direct formation of the alkoxo intermediate without going through a cyclohexyl radical intermediate.

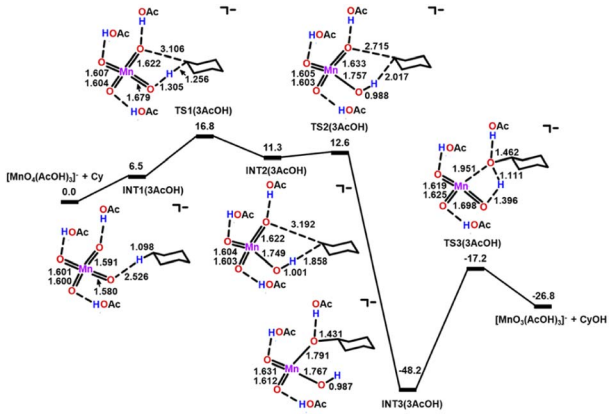

Fig. 9 PES and structures for cyclohexane oxidation by [MnO_4(-AcOH)$_3$]$^-$ at the B3LYP-D3(BJ)/def2-SVPD level. The relative 298 K Gibbs free energies in acetonitrile are given in kcal mol^{-1}.

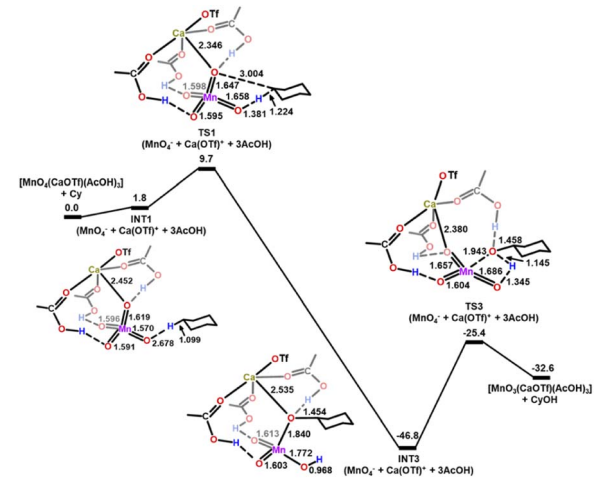

Fig. 11 PES and structures for cyclohexane oxidation by [MnO_4(-CaOTf)(AcOH)$_3$] at the B3LYP-D3(BJ)/def2-SVPD level. The relative 298 K Gibbs free energies in acetonitrile are given in kcal mol^{-1}.

© 2022 The Author(s). Published by the Royal Society of Chemistry

Open Access Article. Published on 13 September 2022. Downloaded on 2/12/2026 9:22:40 AM. This article is licensed under a Creative Commons Attribution-NonCommercial 3.0 Unported Licence.

Table 2 Activation barrier ($\Delta G^{\ddagger}_{298}$, kcal mol^{-1}) for the oxidation of c-C_6H_{12} by RuO_4^- and MnO_4^- under various conditions

	RuO_4^-	MnO_4^-
No additive	26.8	22.7
AcOH	15.2	16.8
Ca^{2+}	18.5	12.7
AcOH + Ca^{2+}	10.8	9.7

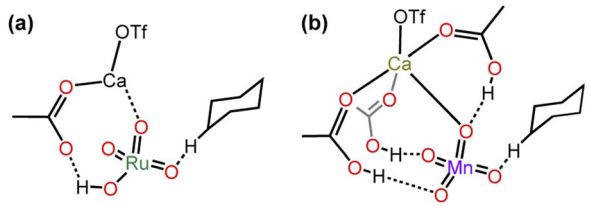

Fig. 12 Structures of the intermediates (a) RuO_4^-/AcOH/Ca(OTf)$_2$ and (b) MnO_4^-/AcOH/Ca(OTf)$_2$.

$\Delta G^{\ddagger}_{298}$ was also determined experimentally by performing kinetics studies at 20–50 °C. From the Arrhenius plot $\Delta G^{\ddagger}_{298}$ was found to be 10.4 ± 0.6 kcal mol^{-1}, in agreement with the calculated value (Fig. S12†).

We have also calculated the TS barrier heights for hydroxylation *via* a rebound mechanism and they are higher than those of the TS forming the alkoxo intermediate by 2–3.4 kcal mol^{-1} (Table S1†).

Activating effects of Ca^{2+}/AcOH on MnO_4^- *vs.* RuO_4^-

Although MnO_4^- and RuO_4^- are isostructural with similar E^0 (0.56 V and 0.59 V, respectively), there is a great difference in the basicity of their oxo ligands; MnO_4^- is a weak base (pK_a of $HMnO_4$ is −2.25),[30] whereas RuO_4^- is a much stronger base. Although the pK_a of $HRuO_4$ is not known, RuO_4^- is readily protonated by weak acids such as AcOH to give [RuO_3(OH)(AcO)$^-$], which readily undergoes HAT with c-C_6H_{12} with a barrier that is lower than that of RuO_4^- by >10 kcal mol^{-1} (Table 2).[25] In contrast, MnO_4^- is not protonated by AcOH. Nevertheless, AcOH can still exert a moderate activating effect on HAT by MnO_4^- through H-bonding with the oxo ligands, with the activation barrier lowered by 6 kcal mol^{-1} compared with MnO_4^- alone. On the other hand, Ca^{2+} has a higher activating effect on MnO_4^- than on RuO_4^- (lowering of the barrier is 10 *vs.* 8 kcal mol^{-1}). Remarkably, for both complexes the presence of AcOH and Ca^{2+} together shows a similar synergistic activating effect, resulting in a lowering of the HAT barrier by 16 and 13 kcal mol^{-1} for RuO_4^- and MnO_4^-, respectively. DFT calculations show that Ca(II) forms a MO_4^-/AcOH/Ca(II) active intermediate by binding to AcO^-/AcOH and an oxo ligand (Fig. 12).

Conclusions

In conclusion, we have demonstrated synergistic activating effects of a weak Brønsted acid such as acetic acid and a weak Lewis acid such as Ca^{2+} on MnO_4^-. Although MnO_4^- is rather non-basic, it can readily be activated by AcOH + Ca^{2+} toward HAT of c-C_6H_{12}, resulting in a lowering of the barrier by 13 kcal mol^{-1}. Remarkably, such a cooperative effect on MnO_4^- is similar to that on RuO_4^-, despite a great difference in the basicity of the two metal-oxo species, which should lead to vastly different affinities toward acids. Our studies suggest that such a synergistic activation is a general phenomenon which may occur in various other metal-oxo species.

The combination of a weak Brønsted and a weak Lewis acid is a potentially useful strategy for the activation of a metal-oxo species toward oxidation of various organic compounds, particularly for substrates that may contain functional groups that are sensitive to strong acids. It is possible that this synergistic activating effect on metal-oxo species may also occur in biological systems, where only relatively mild Brønsted acids and Lewis acids (metal ions) are present.

Data availability

The datasets supporting this article have been uploaded as part of the ESI.†

Author contributions

C. K. M. designed and carried out the experiments, analysed the data and wrote the manuscript. T. C. L. designed the experiments and wrote the manuscript. H. S. performed the experiments and helped in the analysis of the data and preparation of the manuscript. L. C., Y. P. and K. C. L. performed computational studies and wrote the manuscript.

Conflicts of interest

There are no conflicts to declare.

Note added after first publication

This article replaces the version published on 26/09/2022, which contained errors in the position of the equilibrium constants in equations 1, 4, 7 and 8.

Acknowledgements

This work was supported by the NSFC/RGC Joint Research Scheme (N_CityU111/20) and the Laboratory for Synthetic Chemistry and Chemical Biology Limited, LSCCB. The computational studies were carried out using the computational facilities at Burgundy at City University of Hong Kong.

References

1 M. Sono, M. P. Roach, E. D. Coulter and J. H. Dawson, *Chem. Rev.*, 1996, **96**, 2841–2887.
2 B. Meunier, S. P. de Visser and S. Shaik, *Chem. Rev.*, 2004, **104**, 3947–3980.
3 T. L. Poulos, *Chem. Rev.*, 2014, **114**, 3919–3962.

Open Access Article. Published on 13 September 2022. Downloaded on 2/12/2026 9:22:40 AM. This article is licensed under a Creative Commons Attribution-NonCommercial 3.0 Unported Licence.

4 X. P. Zhang, A. Chandra, Y. M. Lee, R. Cao, K. Ray and W. Nam, *Chem. Soc. Rev.*, 2021, **50**, 4804–4811.
5 Y. Y. Liu and T. C. Lau, *J. Am. Chem. Soc.*, 2019, **141**, 3755–3766.
6 T. Devi, Y. M. Lee, W. Nam and S. Fukuzumi, *Coord. Chem. Rev.*, 2020, **410**, 213219.
7 K. N. Ferreira, T. M. Iverson, K. Maghlaoui, J. Barber and S. Iwata, *Science*, 2004, **303**, 1831–1838.
8 Y. Umena, K. Kawakami, J. R. Shen and N. Kamiya, *Nature*, 2011, **473**, 55–U65.
9 H. X. Du, P. K. Lo, Z. M. Hu, H. J. Liang, K. C. Lau, Y. N. Wang, W. W. Y. Lam and T. C. Lau, *Chem. Commun.*, 2011, **47**, 7143–7145.
10 R. A. Baglia, C. M. Krest, T. Yang, P. Leeladee and D. P. Goldberg, *Inorg. Chem.*, 2016, **55**, 10800–10809.
11 J. Chen, Y. M. Lee, K. M. Davis, X. Wu, M. S. Seo, K. B. Cho, H. Yoon, Y. J. Park, S. Fukuzumi, Y. N. Pushkar and W. Nam, *J. Am. Chem. Soc.*, 2013, **135**, 6388–6391.
12 H. Yoon, Y. M. Lee, X. Wu, K. B. Cho, R. Sarangi, W. Nam and S. Fukuzumi, *J. Am. Chem. Soc.*, 2013, **135**, 9186–9194.
13 Z. Q. Chen, L. Yang, C. Choe, Z. N. Lv and G. C. Yin, *Chem. Commun.*, 2015, **51**, 1874–1877.
14 C. Choe, L. Yang, Z. A. Lv, W. L. Mo, Z. Q. Chen, G. X. Li and G. C. Yin, *Dalton Trans.*, 2015, **44**, 9182–9192.
15 Y. Morimoto, H. Kotani, J. Park, Y. M. Lee, W. Nam and S. Fukuzumri, *J. Am. Chem. Soc.*, 2011, **133**, 403–405.
16 J. Park, Y. Morimoto, Y. M. Lee, W. Nam and S. Fukuzumi, *J. Am. Chem. Soc.*, 2011, **133**, 5236–5239.
17 S. M. Yiu, W. L. Man and T. C. Lau, *J. Am. Chem. Soc.*, 2008, **130**, 10821–10827.
18 W. W. Y. Lam, S.-M. Yiu, J. M. N. Lee, S. K. Y. Yau, H.-K. Kwong, T.-C. Lau, D. Liu and Z. Lin, *J. Am. Chem. Soc.*, 2006, **128**, 2851–2858.
19 T.-C. Lau, Z.-B. Wu, Z.-L. Bai and C.-K. Mak, *J. Chem. Soc., Dalton Trans.*, 1995, 695–696.
20 T. Devi, Y. M. Lee, W. Nam and S. Fukuzumi, *J. Am. Chem. Soc.*, 2018, **140**, 8372–8375.
21 T. Devi, Y. M. Lee, W. Nam and S. Fukuzumi, *J. Am. Chem. Soc.*, 2020, **142**, 365–372.
22 E. Y. Tsui and T. Agapie, *Proc. Natl. Acad. Sci. U. S. A.*, 2013, **110**, 10084–10088.
23 E. Y. Tsui, R. Tran, J. Yano and T. Agapie, *Nat. Chem.*, 2013, **5**, 293–299.
24 M. M. Najafpour, T. Ehrenberg, M. Wiechen and P. Kurz, *Angew. Chem., Int. Ed.*, 2010, **49**, 2233–2237.
25 G. Chen, L. Ma, P. K. Lo, C. K. Mak, K. C. Lau and T. C. Lau, *Chem. Sci.*, 2021, **12**, 632–638.
26 K. A. Gardner, L. L. Kuehnert and J. M. Mayer, *Inorg. Chem.*, 1997, **36**, 2069–2078.
27 S. J. Hawkes, *J. Chem. Educ.*, 1996, **73**, 516–517.
28 D. G. Lee and J. F. Perez-Benito, *J. Org. Chem.*, 1988, **53**, 5725–5728.
29 M. C. Biesinger, B. P. Payne, A. P. Grosvenor, L. W. M. Lau, A. R. Gerson and R. S. C. Smart, *Appl. Surf. Sci.*, 2011, **257**, 2717–2730.
30 N. Bailey, A. Carrington, K. A. K. Lott and M. C. R. Symons, *J. Chem. Soc.*, 1960, 290–297.

© 2022 The Author(s). Published by the Royal Society of Chemistry